ChemPubSoc Europe

DOI: 10.1002/open.201700083

Open Access ChemistryOPEN Full Papers

Third-Order Nonlinear Optical Properties of One-Dimensional Quinoidal Oligothiophene Derivatives Involving Phenoxyl Groups

Ryohei Kishi,*[a] Tsubasa Katsurayama,[a] Shoki Ochi,[a] Akihiro Makino,[a] Naoyuki Matsushita,[a] Michika Saito,[a] Takanori Nagami,[a] Jun-ya Fujiyoshi,[a] and Masayoshi Nakano*[a, b]

The diradical characters (y) and third-order nonlinear optical (NLO) properties of open-shell quinoidal oligothiophene derivatives with phenoxyl groups, and the corresponding reduced (hydrogenated)-state oligomers, are investigated by using the broken-symmetry density functional theory method. The oxidized (dehydrogenated) states are predicted to have an open-shell singlet ground state and their y values increase with the number of units. Static second hyperpolarizabilities (γ) of the open-shell oligomers with intermediate y are shown to be enhanced significantly compared with those of the closed-shell analogues. Furthermore, owing to the effective diradical distances, the γ values of open-shell oligomers are found to exceed that of *s*-indaceno[1,2,3-*cd*;5,6,7-*c'd'*]diphenalene, which is known as an organic molecule with the largest two-photon absorption cross-section in this size of the pure hydrocarbons. This feature extends the range of efficient open-shell third-order NLO materials to a novel class of one-dimensional conjugated oligomers with redox-based high tunability of third-order NLO properties.

1. Introduction

Third-order nonlinear optical (NLO) phenomena have attracted much attention in the fields of materials science and engineering because they can be utilized in the fundamental technologies of future photonics and optoelectronics.[1] To date, organic molecular systems with large second hyperpolarizabilities (γ: third-order NLO property at the molecular level) have been explored as candidates for novel third-order NLO materials.[2–5] In a series of previous studies, we theoretically clarified the fundamental relationship between diradical character (y) and γ for open-shell singlet systems.[6–11] From analysis of the valence configuration interaction (VCI) solutions for the two-site diradical model by using the localized natural orbital (LNO) basis, we derived the analytic expression of dimensionless γ as a function of y [Eq. (1)]:[9–11]

$$\frac{\gamma}{R^4/U^3} = f_\gamma(y, r_K) \tag{1}$$

$$= -\frac{8(1-y)^4}{\left\{1+\sqrt{1-(1-y)^2}\right\}^2\left\{1-2r_K+1/\sqrt{1-(1-y)^2}\right\}^3} + \frac{4(1-y)^2}{\left\{1-2r_K+1/\sqrt{1-(1-y)^2}\right\}^2\left\{1/\sqrt{1-(1-y)^2}\right\}}$$

Here, $r_K = 2K/U$ is twice the direct exchange integral in the LNO basis divided by the effective Coulomb repulsion U, and R is the effective diradical distance. For $r_K = 0$, we found that the function $f_\gamma(y, r_K)$ increases on going from $y = 0$ (closed-shell) to intermediate y, attains a maximum at intermediate y, and then decreases for $y \approx 1$ (pure diradical). From this result, the γ values of open-shell singlet molecules can be enhanced by 1) tuning y to be in the intermediate region to increase $f_\gamma(y, r_K)$, and 2) increasing the effective diradical distance R.[6–12] On the basis of these strategies, third-order NLO properties have been evaluated and measured for several singlet diradical compounds with intermediate y.[13–19] For example, very strong two-photon absorptions (TPAs) of thermally stable *s*-indaceno[1,2,3-*cd*;5,6,7-*c'd'*]diphenalene (IDPL) and dicyclopenta[*b*;*g*]naphthalene[1,2,3-*cd*;6,7,8-*c'd'*]diphenalene (NDPL), with intermediate y, were observed experimentally.[13] The recent development of synthetic techniques has achieved such thermally stable open-

[a] Dr. R. Kishi, T. Katsurayama, S. Ochi, A. Makino, N. Matsushita, M. Saito, T. Nagami, J.-y. Fujiyoshi, Prof. Dr. M. Nakano
Department of Materials Engineering Science
Graduate School of Engineering Science, Osaka University
1–3, Machikaneyama, Toyonaka, Osaka 560-8531 (Japan)
E-mail: rkishi@cheng.es.osaka-u.ac.jp
mnaka@cheng.es.osaka-u.ac.jp

[b] Prof. Dr. M. Nakano
Center for Spintronics Research Network (CSRN)
Graduate School of Engineering Science, Osaka University
Toyonaka, Osaka 560–8531 (Japan)

Supporting Information and the ORCID identification number(s) for the author(s) of this article can be found under https://doi.org/10.1002/open.201700083.

shell polycyclic aromatic hydrocarbons (PAHs).[15,20] In general, however, the chemical synthesis of open-shell PAHs is still known to be a laborious task. Furthermore, for open-shell PAH systems, y usually increases rapidly as the molecular size ($\approx R$) increases, and tends to reach ≈ 1 (pure diradical). A combination of intermediate y and large R for PAHs can be achieved by introducing additional functional groups or by doping with heteroatoms, which usually needs different and/or additional synthetic steps.

On the other hand, synthetic strategies for one-dimensional conjugated linked-oligomers/polymers are considered to be well-established compared with those for open-shell PAHs. Thus, in this study, we focus on quinoidal oligothiophenes (QTs) and their derivatives as candidates for novel one-dimensional open-shell NLO systems, in which both intermediate y and large R conditions are fulfilled (see Figure 1). Several theoretically stable QTs with different terminal functional groups and/or sidechains have been reported to have different open-shell characters.[21–30] Dicyanomethylene-terminated QTs with different backbone structures and sidechains have been synthesized.[22,23,30] These systems are expected to exhibit unique electronic, electrochemical, optical, and magnetic properties; these features are useful in the creation of novel versatile functional materials. Additionally, the introduction of phenoxyl groups is known to be a useful strategy to stabilize the diradical form in the resonance structure.[31,32] Indeed, 2,6-*tert*-butylphenoxyl-terminated QTs (derivatives of **Ox*n*** in Figure 1a) have been synthesized up to n (the number of thiophene rings) = 4.[21,28,29] Lanata et al. examined the third-order NLO properties of a derivative of **Ox2**, which can be obtained by the oxidation (dehydrogenation) of the corresponding reduced (hydrogenated) state system **Red2** (see Figure 1a) with closed-shell aromatic electronic structures.[28] They have mainly focused on the difference in vibrational contribution to the electronic second hyperpolarizabilities (γ^{v}) between **Ox2** and **Red2** because the dehydrogenation of the terminal phenol groups of **Red2** is expected to convert their structural features from aromatic to quinoid. They have also measured the third-harmonic generation (THG) signals for a thin film of **Ox2**.[28] In their paper, however, a comparison of the electronic γ between the oxidized (dehydrogenated) and reduced (hydrogenated) states was not focused on, and thus the y dependence of their third-order NLO properties has not yet been clarified, although recent studies on **Ox1** and **Ox2** have predicted their open-shell singlet ground state (see Figure 1b) and thus unique optical response properties.[26] Herein, therefore, we focus on the relationship between the redox state, chain-length, y, static linear polarizabilities (α), and γ of the one-dimensional π-conjugated oligomers **Ox*n*** and **Red*n*** for $n = 1$–4. From the calculation results, we discuss the applicability of the QTs to novel one-dimensional third-order NLO materials with high tunability of the third-order NLO properties.

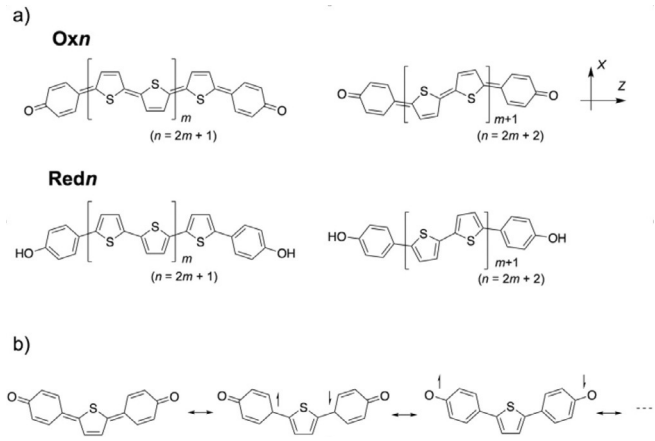

Figure 1. a) Calculated systems **Ox*n*** and **Red*n*** ($m = 0$, 1) and b) resonance structures of open-shell systems **Ox1**. The Cartesian coordinate axis is also shown.

Computational Details

Geometry optimizations were performed at the (U)B3LYP level of approximation. Although the geometric features of QTs are sensitive to the description of electron correlations, the (U)B3LYP optimized geometries are expected to give reliable results for the vibrational spectra of these systems.[23,25–27] The 6-311G* basis set was employed for the geometry optimizations, in which no symmetry constraints were imposed. Subsequently, frequency analysis calculations were performed to obtain a stable local minimum structure. We then set the coordinate axis so that the linear line through the oxygen atoms at each end lie on or is parallel to the z axis.

The diradical character, y,[33,34] is defined as the occupation numbers (n_L) of the lowest unoccupied natural orbital (LUNO), obtained by diagonalizing the one-particle density matrix for the solution of broken-symmetry density functional theory (BS-DFT).[35] The open-shell nature of a molecule can be described by the spatial distribution of the odd-electron density that corresponds to y as $D_y^{odd}(\mathbf{r}) = D_{HONO}(\mathbf{r}) + D_{LUNO}(\mathbf{r})$, in which each of the contributions is defined as $D_k(\mathbf{r}) = min(2 - n_k,\ n_k)\varphi_k^*(\mathbf{r})\varphi_k(\mathbf{r})$.[35,36] The prefactor, $\min(2 - n_k, n_k)$, can be regarded as the probability of the electron of being unpaired in the kth NO $\varphi_k(\mathbf{r})$. Because the trace of the odd-electron density is related to y as $y = \frac{1}{2}\mathrm{Tr}\left[D_y^{odd}(\mathbf{r})\right]$ in the case of the perfect-pairing condition ($n_H + n_L = 2$), the spatial distribution of y is described by the odd-electron density.

Static α and γ are calculated by using the finite-field (FF) approach.[37] In the FF approach, the longitudinal (z axis) components of the static polarizability tensor, $\alpha(=\alpha_{zz})$, and the second hyperpolariability tensor, $\gamma(=\gamma_{zzzz})$ in the B convention[38] are calculated by using the second- and fourth-order numerical differentiation formula [Eq. (2)]:

$$\alpha_{zz} = -\frac{1}{(F^z)^2}\{E(F^z) - 2E(0) + E(-F^z)\} \tag{2}$$

and [Eq. (3)]:

$$\gamma_{zzzz} = \frac{1}{36(F^z)^4}\{E(3F^z) - 12E(2F^z) + 39E(F^z) - 56E(0) + 39E(-F^z) - 12E(-2F^z) + E(-3F^z)\}, \tag{3}$$

in which $E(F^z)$ represents the total energy of a system in the presence of an electric field along the z axis with an amplitude of F^z. The convergence on the total energy was set to 10^{-10} a.u. so that the relative error of the FF γ values becomes within ≈1%. The values of y, α, and γ were calculated by using the long-range corrected (LC-)UBLYP functional[39] with the 6-31G*+p basis set, in which the exponent of diffuse p functions on C (0.0523), N (0.0582), O (0.0719), and S (0.0402) atoms were determined by using the even-tempered method. The range-separating parameter μ for the LC-UBLYP functional was set to 0.33 bohr^{-1} because it has been found to semiquantitatively reproduce γ for open-shell molecules calculated by using the strongly correlated UCCSD(T) method.[40]

To discuss the spatial contributions of electrons to the response properties, we performed the (hyper)polarizability density analysis.[41] From the expansions of the dipole moment and the charge density function $\rho(\mathbf{r}, \mathbf{F})$ in a power series of applied electronic field $\boldsymbol{F}$, α and γ can be expressed by Equation (4a):

$$\alpha_{zz} = -\int r^z \rho_z^{(1)}(\mathbf{r}) d\mathbf{r} \tag{4a}$$

and Equation (4b):

$$\gamma_{zzzz} = -\frac{1}{3!}\int r^z \rho_{zzz}^{(3)}(\mathbf{r}) d\mathbf{r} \tag{4b}$$

in which [Eq. (5a)]:

$$\rho_z^{(1)}(\mathbf{r}) = \left.\frac{\partial \rho(\mathbf{r}, \mathbf{F})}{\partial F^z}\right|_{\mathbf{F}=0} \tag{5a}$$

and [Eq. (5b)]:

$$\rho_{zzz}^{(3)}(\mathbf{r}) = \left.\frac{\partial^3 \rho(\mathbf{r}, \mathbf{F})}{\partial F^z \partial F^z \partial F^z}\right|_{\mathbf{F}=0} \tag{5b}$$

Here, r^z represents the z axis component of the electron coordinate and $\rho_z^{(1)}(\mathbf{r})$ [$\rho_{zzz}^{(3)}(\mathbf{r})$] is referred to as the static α (γ) density. The α (γ) density map represents the relative phase and magnitude of change in the first-order (third-order) charge densities between two spatial points with positive and negative α (γ) densities. The sign of the contribution to α (γ) is positive when the direction from positive to negative α (γ) density coincides with the positive direction of the coordinate axis. The sign becomes negative in the opposite case. The magnitude of the contribution associated with this pair of α (γ) densities is proportional to the density amplitudes multiplied by the distance between them. These calculations were performed by using the Gaussian 09 program package.[42]

To compare dimensionless α and γ of the calculated systems with different chain lengths, we also evaluated the effective diradical distance (R) and the effective Coulomb repulsion (U). R was evaluated from the one-electron transition dipole moment between the HONO and LUNO of the LC-UBLYP NOs, that is, $R = \left|-2\int \varphi_H(\mathbf{r}) \mathbf{r} \varphi_L(\mathbf{r}) d\mathbf{r}\right|$, whereas U was obtained from the direct exchange integral between these NOs (K_{HL}), that is, $U = 2K_{HL} = 2\int \varphi_H(\mathbf{r}_1)\varphi_L(\mathbf{r}_2)\frac{1}{r_{12}}\varphi_L(\mathbf{r}_1)\varphi_H(\mathbf{r}_2) d\mathbf{r}_1 d\mathbf{r}_2$.[25,43] Then, dimensionless α and γ were obtained by using $\alpha/(R^2/U)$ and $\gamma/(R^4/U^3)$, respectively. Because the analytic expressions in terms of y are derived on the basis of the two-electron and two-orbital VCI solutions, we also evaluated $y = y_{CAS}$ obtained by diagonalizing the ground-state density constructed from the two-electron and two-orbital complete active space CI [CASCI(2e,2o)] as a measure of y for the analysis of dimensionless α and γ. These molecular integral evaluations and CASCI calculations were performed by using the GAMESS program package.[44]

2. Results and Discussion

2.1. Geometric Features

Geometric features for the bond-length alternation (BLA) patterns of **Ox*n*** at the (U)B3LYP level of approximation have been discussed in previous studies.[26,27] Here we briefly discuss the optimized geometric parameters of **Ox*n*** and **Red*n*** for n = 1–4. The UB3LYP optimized geometry is found to reduce to the RB3LYP one for **Ox1**. Compounds **Ox*n*** are found to have planar structures with the highest possible symmetries (C_{2v} for **Ox1** and **Ox3**, and C_{2h} for **Ox2**) except for **Ox4**, which has a slightly nonplanar structure. Figure 2 shows the C–C bond

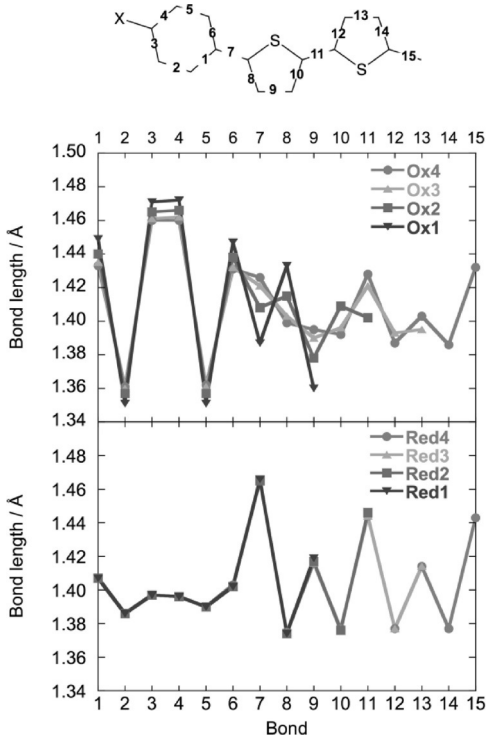

Figure 2. Bond lengths for **Ox*n*** and **Red*n*** and the numbering scheme for each C–C bond.

lengths of the optimized geometries. The BLA of the terminal phenoxyl groups for **Ox*n*** is found to show similar quinoidal pattern for all n, whereas that of the central thiophene part strongly depends on n. Although **Ox1** and **Ox2** exhibit a quinoidal BLA pattern over the whole systems, the central Cα–Cα bond length of **Ox2** is found to be close to 1.4 Å, which lies in between standard single- and double-bond lengths. This indicates that as the chain-length increases, the quinoidal BLA pattern gradually collapses in the central region, and then the aromatic BLA pattern begins to appear. Indeed, the thiophene rings linked to the terminal phenoxyl group for **Ox3** and **Ox4**,

with longer chain lengths, are found to exhibit negligible BLA, and the aromatic pattern clearly appears in the central region. This negligible BLA pattern is predicted to be mainly attributed to the stabilization of the aromatic form in the central region, although the spin-contamination in the BS-DFT solution may somewhat affect the BLA in the present case.[26] Similar results for the chain-length dependence of the BLA pattern were also observed in dicyanomethylene-terminated QTs.[23,25] In summary, the aromaticity of each ring tends to increase on going from the terminal ring to the central ring in **Ox*n***. In contrast, all **Red*n*** are found to have nonplanar structures, which indicates the single-bond nature for all the ring linkers. Namely, the terminal phenol groups of **Red*n*** are found to exhibit negligible BLA, which indicates the aromatic nature of the six-membered rings, and all the thiophene rings exhibit the aromatic BLA pattern regardless of *n*.

2.2. Electronic Structures

The aromaticity of each ring is closely related to the diradical nature of the QT through the quinoid/aromatic resonance structure (see Figure 1b). Calculated *y* values for **Ox*n*** and **Red*n*** are listed in Tables 1 and 2, respectively. From the results, nonzero *y* values are obtained for **Ox*n***, that is, **Ox1** (0.325), **Ox2** (0.656), **Ox3** (0.865), and **Ox4** (0.949), which indicates the open-shell singlet ground state for these systems. The open-shell nature of **Ox*n*** is found to increase as *n* increases, and **Ox4** is expected to have almost pure diradical nature. In contrast, the *y* values for **Red*n*** are calculated to be zero, that is, these systems are closed-shell in the ground state, as expected from Figure 1. These results indicate that the oxidation reactions for **Red*n*** are expected to change their electronic structure from closed-shell to open-shell singlet. Figure 3 shows the spatial distributions of the HONO and LUNO and the odd-electron densities. Judging from the bonding/antibonding characters, the HONO and LUNO of open-shell **Ox*n*** are found to have quinoidal and aromatic features, respectively (see Figure 3a). As *n* increases, the spatial distributions of the HONO and LUNO tend to be localized primarily on the terminal regions. This is understood by the fact that the HONO and LUNO have similar significant distribution on the terminal regions in **Ox4**. The odd-electron densities of **Ox*n*** are primarily distributed not only on the phenoxyl groups but also on the nearest-neighboring thiophene rings, which indicates that unpaired electrons are delocalized over several atomic sites within each terminal region. This feature indicates that the electronic struc-

Table 1. Diradical character *y*, polarizability α, second hyperpolarizability γ, and α/N and γ/N values for **Ox*n*** systems calculated at the LC-(U)BLYP/6-31G*+*p* level of approximation.[a]

	Ox1	Ox2	Ox3	Ox4
N	3	4	5	6
y [–]	0.325	0.656	0.865	0.949
α [a.u.]	711	1080	1314	1523
α/N [a.u.]	237	270	263	254
$r(\alpha/N)$ [–]	1.00	1.14	1.11	1.07
γ [10^4 a.u.]	89.3	422	809	1020
γ/N [10^4 a.u.]	29.8	106	162	170
$r(\gamma/N)$ [–]	1.00	3.54	5.44	5.70
R [a.u.]	10.569	16.466	24.938	33.294
U [a.u.]	0.1064	0.1295	0.1685	0.1924
y_{CAS} [–]	0.115	0.315	0.687	0.882
$\alpha/(R^2/U)$ [–]	0.677	0.516	0.356	0.264
$\gamma/(R^4/U^3)$ [–]	0.0862	0.125	0.100	0.0591

[a] The ratios of α/N and γ/N with respect to those of **Ox1** [$r(\alpha/N)$ and $r(\gamma/N)$], *R*, *U*, and dimensionless α [$\alpha/(R^2/U)$] and γ [$\gamma/(R^4/U^3)$] are also listed.

Table 2. Diradical character *y*, polarizability α and second hyperpolarizability γ, and α/N and γ/N values for **Red*n*** systems calculated at the LC-(U)BLYP/6-31G*+*p* level of approximation.[a]

	Red1	Red2	Red3	Red4
N	3	4	5	6
y [–]	0.000	0.000	0.000	0.000
α [a.u.]	367	541	730	993
α/N [a.u.]	122	135	146	166
$r(\alpha/N)$ [–]	1.00	1.11	1.20	1.36
γ [10^4 a.u.]	9.9	28.4	64.5	113.6
γ/N [10^4 a.u.]	3.3	7.1	12.9	18.9
$r(\gamma/N)$ [–]	1.00	2.15	3.90	5.73
R [a.u.]	5.096	5.654	6.333	6.700
U [a.u.]	0.0461	0.0393	0.0332	0.0278
y_{CAS} [–]	0.008	0.007	0.006	0.004
$\alpha/(R^2/U)$ [–]	0.651	0.665	0.604	0.615
$\gamma/(R^4/U^3)$ [–]	0.0144	0.0169	0.0147	0.0121

[a] The ratios of α/N and γ/N with respect to those of **Red1** [$r(\alpha/N)$ and $r(\gamma/N)$], *R*, *U*, and dimensionless α [$\alpha/(R^2/U)$] and γ [$\gamma/(R^4/U^3)$] are also listed.

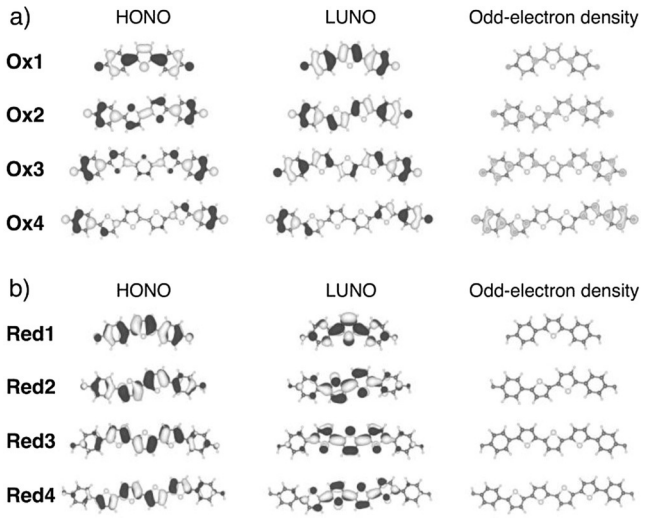

Figure 3. HONO, LUNO, and odd-electron density distributions of a) **Ox*n*** and b) **Red*n***. For NOs, the white/black meshes represent the isosurfaces with contour values of +0.03/−0.03 a.u. For the odd-electron density map, the grey mesh represents the isosurface with a contour value of 0.003 a.u.

ture of **Ox*n*** is described by the resonance structures of the closed-shell quinoid form and plural open-shell aromatic forms in which the positions of radical sites are different from each other. Similar results for the localization of HONO and LUNO were also obtained for dicyanomethylene-terminated QTs with longer chain lengths.[25] In contrast, for **Red*n***, both the HONO and LUNO tend to be localized on the central oligothiophene part as *n* increases. The HONO and LUNO of closed-shell **Red*n*** represent aromatic and quinoidal characters, respectively (see Figure 3b). Of course, no odd-electron density distributions are observed for closed-shell **Red*n***. From this analysis, **Red*n*** and **Ox*n*** are found to be suitable for a direct and fair comparison of the (non)linear optical properties of closed- and open-shell systems because they have the same backbone structures but exhibit different *y* values for a given *n*.

2.3. Polarizabilities (α) and Second Hyperpolarizabilities (γ)

In Tables 1 and 2, the calculation results of α and γ are also summarized. The absolute values of α for open-shell **Ox1** (711 a.u.), **Ox2** (1080 a.u.), **Ox3** (1314 a.u.), and **Ox4** (1523 a.u.) are larger than those of the corresponding closed-shell **Red1** (367 a.u.), **Red2** (541 a.u.), **Red3** (730 a.u.), and **Red4** (993 a.u.). The ratio of α(**Ox*n***)/α(**Red*n***) is found to decrease gradually as *n* increases (α(**Ox*n***)/α(**Red*n***) = 1.94 (*n* = 1), 2.00 (*n* = 2), 1.80 (*n* = 3), 1.53 (*n* = 4)). Thus, the oxidation reaction of **Red*n*** changes their static linear optical properties to some extent within the examined chain length. The chain-length dependence of α (γ) in one-dimensional oligomers is usually discussed by using the α (γ) per unit, that is, α/N (γ/N). Thus, we adopt the total number of five- and six-membered rings as the number of units (*N*), such that $N = n + 2$. The chain-length dependence can be further discussed by examining the increase in the α/N ratio to that of $n = 1$, that is, $r(\alpha/N) = [\alpha/N]/[\alpha/N(n = 1)]$. It is found that the $r(\alpha/N)$ values of **Ox*n*** are slightly larger than 1.0. The ratio takes maximum at **Ox2** (1.14), then slightly decreases with the increase of *n*. This difference is predicted to originate in the intermediate *y* of **Ox2**, which tends to give larger α/N values than those with smaller (**Ox1**) and larger (**Ox3, Ox4**) *y* values. Conversely, the $r(\alpha/N)$ value of **Red*n*** increases monotonically with *n*, and α/N at $n = 4$ becomes 136% of that of $n = 1$. The larger increase in the ratio of α/N in **Red*n*** is also predicted to be caused by the larger conjugation than that of the open-shell singlet systems of **Ox*n*** with similar chain length.[45] In conclusion, the differences in the chain-length dependence of α/N leads to the decrease in α(**Ox*n***)/α(**Red*n***) with *n*.

Next, we move on to the results for γ. The absolute values of γ for **Ox1** (89.3×10^4 a.u.), **Ox2** (422×10^4 a.u.), **Ox3** (809×10^4 a.u.), and **Ox4** (1020×10^4 a.u.) are about one order larger than those of the corresponding closed-shell **Red1** (9.9×10^4 a.u.), **Red2** (28.4×10^4 a.u.), **Red3** (64.5×10^4 a.u.), and **Red4** (113.6×10^4 a.u.). For comparison, the γ value of IDPL was reported to be 175×10^4 a.u. ($y = 0.717$) at the LC-UBLYP/6-31G*//UB3LYP/6-31G* level of approximation.[46] This result indicates that the third-order NLO properties of the one-dimensional open-shell systems **Ox2**–**Ox4** are expected to exceed those of open-shell PAH, IDPL, although, in this study, we employed a larger basis set, 6-31G* + p. As discussed later, this is mainly due to the combination of intermediate *y* and large *R* in the present open-shell one-dimensional systems. The ratios of γ(**Ox*n***)/γ(**Red*n***) as a function of *n* are 9.02 (*n* = 1), 14.9 (*n* = 2), 12.5 (*n* = 3), and 7.12 (*n* = 4), that is, the ratio is enhanced in the intermediate *y* region, the features of which are similar to that in dicyclopenta-fused acenes.[47] From these results, the oxidation (dehydrogenation) reactions for **Red*n*** are expected to enhance their molecular third-order NLO properties drastically.

Again, we examine the γ/N values and the increase in the γ/N ratios for $n = 1$, $r(\gamma/N) = [\gamma/N]/[\gamma/N(n = 1)]$, to investigate the chain-length dependence of γ/N. The value of $r(\gamma/N)$ for **Red*n*** is found to increase monotonically as *n* increases. The value of $r(\gamma/N)$ for **Ox*n*** is found to increase more rapidly than that of **Red*n*** for small *n*, whereas it tends to converge to a value at large values of *n*. As a result, at $n = 4$, the $r(\gamma/N)$ value for both systems becomes close to each other (5.70 for **Ox4** and 5.73 for **Red4**). Almost pure diradical **Ox4** is found to exhibit the largest γ/N value of the calculated systems, whereas the γ/N values of **Ox2** and **A3** are also comparable to that of **Ox4**. We also evaluate the ground-state Mulliken charge distributions for each fragment to clarify the donor-π-donor/acceptor-π-acceptor effect on α and γ of the open-shell systems.[48] For **Ox*n***, the central oligothiophene part of each system is slightly negatively charged, whereas the terminal phenoxyl groups are slightly positively charged (see Figure S1 in the Supporting Information). In the case of closed-shell **Red*n***, the charge separations between the central and terminal parts are found to be significantly enhanced, that is, donor-π-donor character appears in **Red*n***. As a result, the donor-π-donor effects on the enhancement of α and γ in open-shell **Ox*n*** is not considerable in the present case.

To clarify the spatial contributions of electrons to α and γ, the α and γ densities of these systems are illustrated in Figure 4. From the results for **Ox*n***, as *n* increases, positive and negative α densities tend to appear alternately in the central oligothiophene part, and these contributions cancel each other out. However, large positive and negative α density distributions are well separated on the terminal phenoxyl groups, and thus contribute positively to α. In contrast, for **Red*n*** there is no such a large positive contribution of α densities in the terminal regions, although positive and negative α densities with comparable amplitudes are observed alternately over the molecule. In the case of γ for **Ox2**–**Ox4**, positive and negative γ densities with significant amplitudes are distributed on the terminal phenoxyl groups and spatially well separated from each other, which indicates a significant field-induced charge transfer between the terminals, although there are some cancellations of the positive and negative γ densities in the oligothiophene part. In sharp contrast, the amplitudes of γ densities for **Red*n*** are considerably small everywhere in the system compared with those for **Ox*n*** (see Figure 4). The result indicates that the significant field-induced third-order charge transfer in open-shell **Ox*n*** contributes significantly to the enhancement in γ.

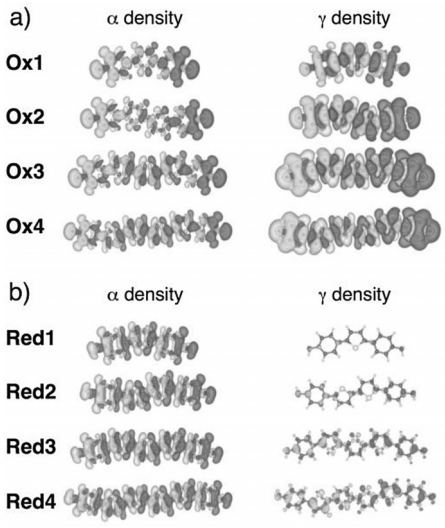

Figure 4. The α and γ density maps for a) **Ox*n*** and b) **Red*n***. The grey/black meshes represent isosurfaces with contour values of +0.05/-0.05 a.u. for α densities and +500/−500 a.u. for γ densities.

The detailed behavior of y dependence of α and γ can be understood by examining dimensionless α ($\alpha/(R^2/U)$) and dimensionless γ ($\gamma/(R^4/U^3)$). Calculated parameters U, R, $\alpha/(R^2/U)$, and $\gamma/(R^4/U^3)$ are listed in Tables 1 and 2. With increasing n, the effective diradical distance R of **Ox*n*** is found to increase rapidly, whereas that of **Red*n*** increases very moderately. We also evaluate the analytic expression of $\alpha/(R^2/U)$ and $\gamma/(R^4/U^3)$ as a function of y [Eq. (6)]:[9–11]

$$\frac{\alpha}{R^2/U} = f_\alpha(y, r_K) = \frac{2\left\{1-\sqrt{1-(1-y)^2}\right\}}{\left\{1-2r_K+1/\sqrt{1-(1-y)^2}\right\}} \quad (6)$$

and Equation (1). In Figure 5, we compare the results of **Ox*n*** and **Red*n*** by using Equations (6) and (1) with $r_K=0$. Note that we employ $y=y_{CAS}$ obtained by using CASCI(2e,2o) calculations with the LC-UBLYP NOs as the horizontal axes for the plots of **Ox*n*** and **Red*n***. Although the y_{CAS} values are small to some extent, the order of the y_{CAS} values of **Ox*n*** are the same as the

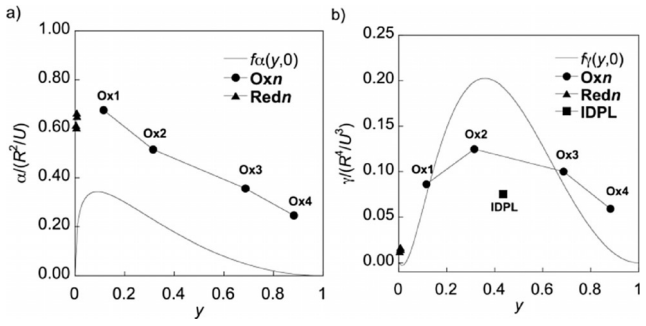

Figure 5. Plots of a) dimensionless $\alpha/(R^2/U)$ and b) dimensionless $\gamma/(R^4/U^3)$ for **Ox*n*** and **Red*n***. The results are compared with the analytic expressions of dimensionless α [Eq. (6)] and γ [Eq. (1)] for $r_K=0$. Values of $y=y_{CAS}$ were used as the horizontal axes for the results of **Ox*n*** and **Red*n***.

original y values evaluated from the LC-UBLYP n_L (see Tables 1 and 2). The analytic result $f_\alpha(y, 0)$ reaches maximum at around $y\approx0.1$, then decreases as y increases. The $\alpha/(R^2/U)$ value for **Ox*n*** is also found to decrease as y increases. This behavior is shown to be in good agreement with the variation in α for the H_2 dissociation model.[8] Although each $\alpha/(R^2/U)$ value for **Ox*n*** is larger by about 0.2 to 0.3 compared with the corresponding analytic result, the decreasing behavior is qualitatively in agreement with that of $f_\alpha(y, 0)$ (see Figure 5a). The discrepancy between them is predicted to originate in the contributions of the orbitals except for the HONO–LUNO pair. From the analysis of the VCI results, the square of the transition dipole moment between the ground (g) and the first allowed excited (e1) states divided by R, that is, $(\mu_{ge1}/R)^2$, is shown to decrease monotonically as y increases,[11] which is a main cause of the decrease in $f_\alpha(y, 0)$. For $\gamma/(R^4/U^3)$, the peak position and the variation in $\gamma/(R^4/U^3)$ with y for **Ox*n*** are similar to those of $f_\gamma(y, 0)$, although the maximum value for **Ox*n*** given at intermediate y (**Ox2**: $y_{CAS}=0.315$) is smaller than that of $f_\gamma(y, 0)$ (see Figure 5b). From the analysis of the VCI results, the enhancement in $\gamma/(R^4/U^3)$ in the intermediate y region is attributed to the increase in the square of the transition dipole moment between the first allowed (e1) and higher-lying forbidden (e2) excited states divided by R, that is, $(\mu_{e1e2}/R)^2$,[11] and the rapid decrease in the excitation energies divided by U for these states, that is, E_{e1}/U and E_{e2}/U. Thus, the y dependencies of these excitation properties are also expected in real **Ox*n*** systems. The qualitative and semiquantitative agreement in the y–α and y–γ plots indicate that the first-order and third-order NLO properties of the present QT systems can be described well by the two-site diradical model [Eqs. (6) and (1)].

Furthermore, we also plotted the results for open-shell PAH, IDPL, in Figure 5b. For IDPL, the (longitudinal tensor component of) absolute γ value is 175×10^4 a.u. at the LC-UBLYP/6-31G* level of approximation, and $y_{CAS}=0.435$, $R=14.807$ a.u. and $U=0.1275$ a.u. by using the LC-UBLYP NOs. Although the $\gamma/(R^4/U^3)$ values of **Ox2**–**Ox4** ($\approx$0.0591–0.125) are similar to that of IDPL (0.0753), the absolute γ values of **Ox2**–**Ox4** (≈422–1020×10^4 a.u.) are much larger than that of IDPL. Because $\gamma=f_\gamma(y, r_K)\times(R^4/U^3)$, the enhancement in the present open-shell one-dimensional systems is considered to be mainly caused by the combination of intermediate y and large R.

In summary, the present open-shell QTs with intermediate y are considered to be promising candidates for efficient third-order NLO molecules from the viewpoint of the feasibility of synthesis and the large amplitudes of third-order response properties. In particular, open-shell **Ox2**–**Ox4** have been shown to exhibit intermediate y, large γ/N, and a considerable γ(**Ox*n***)/γ(**Red*n***) ratio. Furthermore, the third-order NLO properties of the one-dimensional open-shell systems **Ox2**–**Ox4** are expected to be about one order larger than that of open-shell PAH, IDPL, owing to the combination of intermediate y and large R. The synthesis and characterization of third-order NLO properties of **Ox*n*** (**Red*n***) are not only expected to deepen understanding of the y–γ correlation in real systems, but also to contribute to the design of novel open-shell one-dimensional materials for future NLO devices.

3. Conclusions

The redox state and chain-length dependencies of *y*, linear, and third-order NLO properties of quinoidal oligothiophene derivatives with phenoxyl groups have been investigated by using the BS-DFT method. It is found that the oxidations of hydrogenated state systems **Red*n*** drastically changed the ground-state electronic structures from closed-shell to open-shell singlet. Accordingly, the γ values of open-shell **Ox*n*** are enhanced significantly compared with those of **Red*n***. From analysis of the chain length and *y* dependencies of γ/N and dimensionless γ, **Ox2**–**Ox4** systems with intermediate *y* values are expected to be good candidates for a novel class of one-dimensional third-order NLO materials with redox-based high tunability and also as real open-shell molecules employed in experimental investigation of the y–γ correlation. In fact, the calculated γ values of **Ox2**–**Ox4** with intermediate and large *y* are found to be much larger than that of IDPL, for which extraordinarily strong TPA signals were observed experimentally.

To obtain further information on the y–γ correlation in real systems, investigation of the frequency dispersions of dynamic response properties of the QTs is needed. Indeed, enhancement in THG signal from the derivative of **Ox2** was observed experimentally by tuning the incident beam wavelength.[28] In this regard, although the diradical character dependence of the THG spectrum has been clarified for the two-site diradical model,[49] the comparison of the results with those of real molecular systems, such as **Ox2**, is a challenging theme from the viewpoint of verifying the applicability of our design principle "y–γ correlation" derived from a simple theoretical model.

Acknowledgements

This work was supported by JSPS KAKENHI, grant number JP25248007 in Scientific Research (A), grant number JP24109002 in Scientific Research on Innovative Areas "Stimuli-Responsive Chemical Species", grant number JP17H05157 in Scientific Research on Innovative Areas "π-System Figuration", grant number JP26107525 in Scientific Research on Innovative Areas "Sciences of Atomic Layers", and grant number JP26107004 in Scientific Research on Innovative Areas "Photosynergetics". M.N. also thanks King Khalid University for financial support through grant RCAMS/KKU/001-16 under the Research Center for Advanced Materials Science at King Khalid University, Kingdom of Saudi Arabia. Theoretical calculations were partly performed by using Research Center for Computational Science, Okazaki, Japan.

Conflict of Interest

The authors declare no conflict of interest.

Keywords: density functional calculations · diradicals · nonlinear optics · oligomers · redox systems

[1] a) D. Day, M. Gu, A. Smallridge, *Adv. Mater.* **2001**, *13*, 1005 – 1007; b) S. Kawata, Y. Kawata, *Chem. Rev.* **2000**, *100*, 1777 – 1788; c) S. Tao, T. Miyagoe, A. Maeda, H. Matsuzaki, H. Ohtsu, M. Hasegawa, S. Takaishi, M. Yamashita, H. Okamoto, *Adv. Mater.* **2007**, *19*, 2707 – 2710.

[2] P. N. Prasad, D. J. Williams, *Introduction to Nonlinear Optical Effects in Molecules and Polymers*, Wiley, New York, NY, **1990**.

[3] J. L. Brédas, C. Adant, P. Tackx, A. Persoons, B. M. Pierce, *Chem. Rev.* **1994**, *94*, 243 – 278.

[4] B. Champagne, B. Kirtman in *Handbook of Advanced Electronic and Photonic Materials and Devices*, (Ed.: H. S. Nalwa), *Vol. 9*, Academic Press, New York, NY, **2001**, Chap. 2, p. 63.

[5] M. G. Papadopoulos, A. J. Sadlej, J. Leszczynski, *Non-Linear Optical Properties of Matter—From Molecules to Condensed Phases*, Springer, Dordrecht, **2006**.

[6] M. Nakano, H. Nagao, K. Yamaguchi, *Phys. Rev. A* **1997**, *55*, 1503 – 1513.

[7] M. Nakano, R. Kishi, T. Nitta, T. Kubo, K. Nakasuji, K. Kamada, K. Ohta, B. Champagne, E. Botek, K. Yamaguchi, *J. Phys. Chem. A* **2005**, *109*, 885 – 891.

[8] M. Nakano, R. Kishi, S. Ohta, A. Takebe, H. Takahashi, S. Furukawa, T. Kubo, Y. Morita, N. Nakasuji, K. Yamaguchi, K. Kamada, K. Ohta, B. Champagne, E. Botek, *J. Chem. Phys.* **2006**, *125*, 074113 – 074119.

[9] M. Nakano, R. Kishi, S. Ohta, H. Takahashi, T. Kubo, K. Kamada, K. Ohta, E. Botek, B. Champagne, *Phys. Rev. Lett.* **2007**, *99*, 033001 – 033004.

[10] a) M. Nakano, *Excitation Energies and Properties of Open-Shell Singlet Molecules*, Springer, Berlin, **2014**; b) M. Nakano, *Top. Curr. Chem.* **2017**, *375*, 47 – 113.

[11] a) M. Nakano, B. Champagne, *J. Phys. Chem. Lett.* **2015**, *6*, 3236 – 3256; b) M. Nakano, B. Champagne, *WIREs Comput. Mol. Sci.* **2016**, *6*, 198 – 210; c) M. Nakano, *Chem. Rec.* **2017**, *17*, 27 – 62.

[12] H. Fukui, M. Nakano, Y. Shigeta, B. Champagne, *J. Phys. Chem. Lett.* **2011**, *2*, 2063 – 2066.

[13] K. Kamada, K. Ohta, T. Kubo, A. Shimizu, Y. Morita, K. Nakasuji, R. Kishi, S. Ohta, S. Furukawa, H. Takahashi, M. Nakano, *Angew. Chem. Int. Ed.* **2007**, *46*, 3544 – 3546; *Angew. Chem.* **2007**, *119*, 3614 – 3616.

[14] H. Kishida, K. Hibino, A. Nakamura, D. Kato, J. Abe, *Thin Solid Films* **2010**, *519*, 1028 – 1030.

[15] Y. Li, W.-K. Heng, B. S. Lee, N. Aratani, J. L. Zafra, N. Bao, R. Lee, Y. M. Sung, Z. Sun, K.-W. Huang, R. D. Webster, J. T. López Navarrete, D. Kim, A. Osuka, J. Casado, J. Ding, J. Wu, *J. Am. Chem. Soc.* **2012**, *134*, 14913 – 14922.

[16] Z. Zeng, Y. M. Sung, N. Bao, D. Tan, R. Lee, J. L. Zafra, B. S. Lee, M. Ishida, J. Ding, J. T. Lopez Navarrete, Y. Li, W. Zeng, D. Kim, K.-W. Huang, R. D. Webster, J. Casado, J. Wu, *J. Am. Chem. Soc.* **2012**, *134*, 14513 – 14525.

[17] Z. Zeng, M. Ishida, J. L. Zafra, X. Zhu, Y. M. Sung, N. Bao, R. D. Webster, B. S. Lee, R.-W. Li, W. Zeng, Y. Li, C. Chi, J. T. López Navarrete, J. Ding, J. Casado, D. Kim, J. Wu, *J. Am. Chem. Soc.* **2013**, *135*, 6363 – 6371.

[18] H. S. Quah, W. Chen, M. K. Schreyer, H. Yang, M. W. Wong, W. Ji, J. J. Vittal, *Nat. Commun.* **2015**, *6*, 7954 – 7957.

[19] K. Kamada, S. Fuku-en, S. Minamide, K. Ohta, R. Kishi, M. Nakano, H. Matsuzaki, H. Okamoto, H. Higashikawa, K. Inoue, S. Kojima, Y. Yamamoto, *J. Am. Chem. Soc.* **2013**, *135*, 232 – 241.

[20] a) T. Kubo, A. Shimizu, M. Sakamoto, M. Uruichi, K. Yakushi, M. Nakano, D. Shiomi, K. Sato, T. Takui, Y. Morita, K. Nakasuji, *Angew. Chem. Int. Ed.* **2005**, *44*, 6564 – 6568; *Angew. Chem.* **2005**, *117*, 6722 – 6726; b) A. Konishi, Y. Hirao, M. Nakano, A. Shimizu, E. Botek, B. Champagne, D. Shiomi, K. Sato, T. Takui, K. Matsumoto, H. Kurata, T. Kubo, *J. Am. Chem. Soc.* **2010**, *132*, 11021 – 11023; c) S. Nobusue, H. Miyoshi, A. Shimizu, I. Hisaki, K. Fukuda, M. Nakano, Y. Tobe, *Angew. Chem. Int. Ed.* **2015**, *54*, 2090 – 2094; *Angew. Chem.* **2015**, *127*, 2118 – 2122; d) G. E. Rudebusch, J. L. Zafra, K. Jorner, K. Fukuda, J. L. Marshall, I. Arrechea-Marcos, G. L. Espejo, R. P. Ortiz, C. J. Gómez-García, L. N. Zakharov, M. Nakano, H. Ottosson, J. Casado, M. M. Haley, *Nat. Chem.* **2016**, *8*, 753 – 759.

[21] K. Takahashi, T. Suzuki, *J. Am. Chem. Soc.* **1989**, *111*, 5483 – 5485.

[22] T. Takahashi, K. Matsuoka, K. Takimiya, T. Otsubo, Y. Aso, *J. Am. Chem. Soc.* **2005**, *127*, 8928 – 8929.

[23] R. P. Ortiz, J. Casado, S. Rodrígues González, V. Hernández, J. T. Lopez Navarrete, P. M. Viruela, E. Ortí, K. Takimiya, T. Otsubo, *Chem. Eur. J.* **2010**, *16*, 470 – 484.

[24] J. Casado, R. P. Ortiz, J. T. Lopez Navarrete, *Chem. Soc. Rev.* **2012**, *41*, 5672 – 5686.

[25] a) R. Kishi, M. Dennis, K. Fukuda, Y. Murata, K. Morita, H. Uenaka, M. Nakano, *J. Phys. Chem. C* **2013**, *117*, 21498 – 21508; b) R. Kishi, S. Ochi, S.

Izumi, A. Makino, T. Nagami, J. Fujiyoshi, N. Matsushita, M. Saito, M. Nakano, *Chem. Eur. J.* **2016**, *22*, 1493 – 1500.
[26] a) D. Fazzi, E. V. Canesi, F. Negri, C. Bertarelli, C. Castiglioni, *ChemPhysChem* **2010**, *11*, 3685 – 3695; b) S. Di Motta, F. Negri, D. Fazzi, C. Castiglioni, E. Valeria Canesi, *J. Phys. Chem. Lett.* **2010**, *1*, 3334 – 3339.
[27] M. Kertesz, C. H. Choi, S. J. Yang, *Chem. Rev.* **2005**, *105*, 3448 – 3481.
[28] M. Lanata, C. Bertarelli, M. C. Gallazzi, A. Bianco, M. Del Zoppo, G. Zerbi, *Synth. Met.* **2003**, *138*, 357 – 362.
[29] K. Takahashi, A. Gunji, K. Yanagi, M. Miki, *J. Org. Chem.* **1996**, *61*, 4784 – 4792.
[30] T. Mori, N. Yanai, I. Osaka, K. Takimiya, *Org. Lett.* **2014**, *16*, 1334 – 1337.
[31] K. Zhang, K.-W. Huang, J. Li, J. Luo, C. Chi, J. Wu, *Org. Lett.* **2009**, *11*, 4854 – 4857.
[32] A. Ueda, S. Nishida, K. Fukui, T. Ise, D. Shiomi, K. Sato, T. Takui, K. Nakasuji, Y. Morita, *Angew. Chem. Int. Ed.* **2010**, *49*, 1678 – 1682; *Angew. Chem.* **2010**, *122*, 1722 – 1726.
[33] E. F. Hayes, A. K. Q. Siu, *J. Am. Chem. Soc.* **1971**, *93*, 2090 – 2091.
[34] K. Yamaguchi, T. Fueno, H. Fukutome, *Chem. Phys. Lett.* **1973**, *22*, 461 – 465.
[35] M. Head-Gordon, *Chem. Phys. Lett.* **2003**, *372*, 508 – 511.
[36] M. Nakano, H. Fukui, T. Minami, K. Yoneda, Y. Shigeta, R. Kishi, B. Champagne, E. Botek, T. Kubo, K. Ohta, K. Kamada, *Theor. Chem. Acc.* **2011**, *130*, 725.
[37] H. D. Cohen, C. C. J. Roothaan, *J. Chem. Phys.* **1965**, *43*, S34 – S39.
[38] A. Willetts, J. E. Rice, D. M. Burland, D. P. Shelton, *J. Chem. Phys.* **1992**, *97*, 7590 – 7599.
[39] H. Iikura, T. Tsuneda, T. Yanai, K. Hirao, *J. Chem. Phys.* **2001**, *115*, 3540 – 3545.
[40] R. Kishi, S. Bonness, K. Yoneda, H. Takahashi, M. Nakano, E. Botek, B. Champagne, T. Kubo, K. Kamada, K. Ohta, T. Tsuneda, *J. Chem. Phys.* **2010**, *132*, 094107 – 094111.
[41] M. Nakano, I. Shigemoto, S. Yamada, K. Yamaguchi, *J. Chem. Phys.* **1995**, *103*, 4175 – 4191.
[42] Gaussian 09, Revision B.01, M. J. Frisch, G. W. Trucks, H. B. Schlegel, G. E. Scuseria, M. A. Robb, J. R. Cheeseman, G. Scalmani, V. Barone, B. Mennucci, G. A. Petersson, H. Nakatsuji, M. Caricato, X. Li, H. P. Hratchian, A. F. Izmaylov, J. Bloino, G. Zheng, J. L. Sonnenberg, M. Hada, M. Ehara, K. Toyota, R. Fukuda, J. Hasegawa, M. Ishida, T. Nakajima, Y. Honda, O. Kitao, H. Nakai, T. Vreven, J. A. Montgomery, Jr., J. E. Peralta, F. Ogliaro, M. Bearpark, J. J. Heyd, E. Brothers, K. N. Kudin, V. N. Staroverov, R. Kobayashi, J. Normand, K. Raghavachari, A. Rendell, J. C. Burant, S. S. Iyengar, J. Tomasi, M. Cossi, N. Rega, J. M. Millam, M. Klene, J. E. Knox, J. B. Cross, V. Bakken, C. Adamo, J. Jaramillo, R. Gomperts, R. E. Stratmann, O. Yazyev, A. J. Austin, R. Cammi, C. Pomelli, J. W. Ochterski, R. L. Martin, K. Morokuma, V. G. Zakrzewski, G. A. Voth, P. Salvador, J. J. Dannenberg, S. Dapprich, A. D. Daniels, Ö. Farkas, J. B. Foresman, J. V. Ortiz, J. Cioslowski, D. J. Fox, Gaussian, Inc., Wallingford CT, **2009**.
[43] Y. Inoue, T. Yamada, B. Champagne, M. Nakano, *Chem. Phys. Lett.* **2013**, *570*, 75 – 79.
[44] M. W. Schmidt, K. K. Baldridge, J. A. Boatz, S. T. Elbert, M. S. Gordon, J. H. Jensen, S. Koseki, N. Matsunaga, K. A. Nguyen, S. J. Su, T. L. Windus, M. Dupuis, J. A. Montgomery, *J. Comput. Chem.* **1993**, *14*, 1347.
[45] M. Nakano, A. Takebe, R. Kishi, S. Ohta, M. Nate, T. Kubo, K. Kamada, K. Ohta, B. Champagne, E. Botek, H. Takahashi, S. Furukawa, Y. Morita, K. Nakasuji, *Chem. Phys. Lett.* **2006**, *432*, 473 – 479.
[46] M. Nakano, T. Minami, K. Yoneda, S. Muhammad, R. Kishi, Y. Shigeta, T. Kubo, L. Rougier, B. Champagne, K. Kamada, K. Ohta, *J. Phys. Chem. Lett.* **2011**, *2*, 1094 – 1098.
[47] S. Motomura, M. Nakano, H. Fukui, K. Yoneda, T. Kubo, R. Carion, B. Champagne, *Phys. Chem. Chem. Phys.* **2011**, *13*, 20575 – 20583.
[48] K. Fukuda, M. Nakano, *J. Phys. Chem. A* **2014**, *118*, 3463 – 3471.
[49] M. Nakano, B. Champagne, *Theor. Chem. Acc.* **2015**, *134*, 231-239.

Received: April 29, 2017
Version of record online July 3, 2017

